Int J Coal Sci Technol (2021) 8(3):383–393
https://doi.org/10.1007/s40789-021-00445-1

Key CO_2 capture technology of pure oxygen exhaust gas combustion for syngas-fueled high-temperature fuel cells

Hanlin Wang[1] · Qilong Lei[2] · Pingping Li[1] · Changlei Liu[2] · Yunpeng Xue[1] · Xuewei Zhang[2] · Chufu Li[1] · Zhibin Yang[3]

Received: 3 June 2020 / Revised: 28 December 2020 / Accepted: 4 June 2021 / Published online: 3 July 2021

Abstract Integrated gasification fuel cells (IGFCs) integrating high-temperature solid oxide fuel cell technology with CO_2 capture processes represents highly-efficient power systems with negligible CO_2 emissions. Flame burning with pure oxygen is an ideal method for fuel cell exhaust gas treatment, and this report describes experimental and numerical studies regarding an oxy-combustor for treating the exhaust gas of a 10 kW IGFC system anode. The applied simulation method was verified based on experiments, and the key performance indices of the combustor were studied under various conditions. It was determined that 315 K was the ideal condensation temperature to obtain flame stability. Under these pure oxygen flame burning conditions, CO was almost completely converted, and the dry mole fraction of CO_2 after burning was $\geq$ 0.958 when there was up to 5% excess O_2. Overall, 5% excess O_2 was recommended to maximize CO_2 capture and promote other environmental considerations. Additionally, the optimal tangential fuel jet angle to control the liner temperature was approximately 25°. The total fuel utilization had to be high enough to maintain the oxygen flame temperature of the anode exhaust gas below 1800 K to ensure that the system was environmentally friendly. The results presented herein have great value for designing IGFCs coupled with CO_2 capture systems.

Keywords Integrated gasification fuel cell system · Solid oxide fuel cell · Anode exhaust gas treatment · CO_2 capture · Oxy-combustion

1 Introduction

To counteract the increasing consumption of non-renewable resources, it is necessary to develop higher-efficiency power systems, because continued fossil fuel combustion contributes to detrimental greenhouse effects. Integrated gasification fuel cell (IGFC) technology (Al-Khori et al. 2020) provides a new approach to designing enhanced power systems. Compared with traditional coal-burning power generators, these systems theoretically perform with higher efficiency. Solid oxide fuel cell (SOFC) technologies could be suitable for IGFCs because they can accommodate a wide range of fuels and can be fed directly with syngas (Wu et al. 2020). Moreover, coupling such SOFC-based IGFC systems with simple CO_2 capturing processes could enable power generation while releasing negligible greenhouse gases (i.e., CO_2), which would incur lower energy penalties and require lower costs relative to conventional methods (Thallam-Thattai et al. 2017). Carbon in the anode exhaust gas must be collected to achieve a high CO_2 capture rate. Generally, SOFCs with high fuel utilization percentages (Pirasaci 2019) accomplish CO_2 capture. For some small systems involving high-fuel-efficiency fuel cells (e.g., the SOLIDpower Company's BlueGEN system), fuel mass flows through the stacks in a single direction (Ferreira et al. 2019), thus simplifying the system. Alternatively, CO_2 can be collected using more

✉ Hanlin Wang
hanlin.wang.a@chnenergy.com.cn

[1] National Institute of Clean and Low-Carbon Energy, Beijing 102211, China

[2] Shenhua New Energy Company, Ltd., Beijing 100007, China

[3] China University of Mining and Technology, Beijing 100083, China

complex system designs. In some cases, anode exhaust gas looping through ejectors has been implemented to enhance fuel utilization, while simultaneously increasing the exhaust's CO_2 density (Wang et al. 2020). For SOFC systems, a certain amount of steam must be blended with the fuel before it enters the stacks to avoid carbon formation or to promote the reforming reaction for systems fueled by CH_4. In systems employing anode looping, steam is provided by the anode exhaust gas, but for anode single-pass systems, such as BlueGEN, some extra steam is imported directly. Different system designs, fuel components, and fuel utilization ratios may lead to variations in the composition of exhaust gas. Therefore, the exhaust gas treatment system must demonstrate effective performance for a relatively wide range of species to ensure suitable system adaption.

Approximately 10%–15% of the combustible components (i.e., primarily CO and H_2) may still remain in exhaust gas, corresponding to a calorific value of 2–3 MJ/Nm^3. In addition to CO_2 capture, further processes are needed to enhance waste heat utilization and fulfill environmental requirements. Ideally, exhaust gas should be completely oxidized to CO_2 and H_2O. Spallina et al. (2018) proposed a chemical looping combustion method to deal with exhaust gas. In this approach, anode exhaust gas was imported to a fuel reactor, where it was looped through ejectors, and then exhaust gas reacted with the cathode inlet air via an oxidizing carrier. The inlet air was heated to 730 °C by an exothermic oxidation reaction before entering the cathode chamber. Implementing these ejectors increased the difficulty in terms of controlling the flow, and chemical looping systems can be expensive. Furthermore, this strategy still may not attain the desired CO_2 capture rate.

Oxy-combustion has been verified as an effective method for concentrating CO_2 in some traditional power systems (Francisco et al. 2016). Compared with air combustion, no extra impurities (e.g., N_2) are imported during the process, which may decrease the capture rate and increase the compression energy required to pressurize the captured CO_2 for storage. For IGFC applications, pure O_2 could easily be obtained from air separators used in the coal gasification process, thus facilitating oxy-combustion. To achieve exhaust gas oxy-combustion, a detailed combustor structure and exhaust gas handling process must be designed.

Catalytic oxy-combustion is often employed to deal with CO pollution in power system exhaust gas. Chen et al. (2019) showed that TiO_2-CuO was an effective catalyst for treating exhaust gas containing 1.5% CO. If the catalytic specific surface area was sufficient, the conversion could reach over 90% in seven hours. Han et al. (2016) demonstrated that nickel oxide catalysts could combust exhaust gas with a CO content of $< 1\%$ by volume at various temperatures; the optimal temperature was 600 °C for a lab-scale system, and no catalyst deactivation was observed during CO oxidation over 720 min. Dey et al. (2020) proposed a detailed catalytic combustor for CO when testing the activity of a Pt catalyst with a porous catalyst bed to increase its specific surface area. Most catalysts are designed to deal with exhaust gas containing CO in concentrations $< 1\%$ by volume, meaning that such catalysts may be suitable for handling exhaust gas containing CO as a pollutant. However, SOFC exhaust gas contains far more CO and H_2, and the gas flow rate is often larger than a lab-scale test. These factors may lead to a high local combustion temperature, which would be harmful to the catalyst's activity. A sufficient specific surface area is required for efficient catalytic combustion, which makes it difficult to scale-up the burner. More researches are needed on catalyst life for long term system design. The pressure of the anode gas should be strictly limited because high-pressure gas is detrimental to the fuel cell seals, while a low exhaust gas pressure may not be sufficient for infiltrating the porous catalyst bed. These aspects introduce challenges in terms of applying catalytic oxy-combustion in practical systems.

Direct pure oxygen flame burning represents another way to treat anode exhaust gas, and this method can almost fully convert CO to CO_2. The main characteristics of exhaust gas are its extremely high moisture content and its low calorific value; these features hinder the flame stability and ignition, respectively. Ning et al. (2018) reported that water vapor and carbon dioxide increased the ignition temperature of an H_2/O_2 flame and had some additional negative effects. These results indicated that the anode exhaust gas should be cooled and dried prior to flame combustion. Recent studies have confirmed that a pure oxygen flame can remain steady under an extremely low equivalence ratio (especially for H_2-enriched fuel), meaning that it might demonstrate good performance for low-calorific exhaust gas. Rashwan et al. (2017) showed that oxygen partially premixed with a natural gas flame could remain steady for equivalence ratios ranging from 0.7 to 1.1. Imteyaz et al. (2018) reported similar results regarding H_2-enriched premixed methane/oxygen combustion. Additionally, they showed that H_2 could reduce the lower limit of the equivalence ratio to 0.2. Li et al. (2018) obtained a stable oxy-methane premixed flame when the O_2 mole fraction ranged from 0.25 to 1.0, and further observed that its stability increased as the O_2 mole fraction increased. An excessive amount of O_2 in this case decreased the CO_2 concentration, although it improved the flame stability. Ilbas et al. (2019) numerically and experimentally studied the oxy-combustion of low-calorific syngas and found that an oxygen flame could burn out almost

all of the CO content. However, flame burning may cause problems regarding NO_x emissions. Pollutant emission is related to flame temperature and burner design, so pollutants must be taken into consideration when developing such power systems because acidic gas may be harmful to the environment as well as to the systems themselves.

According to the literature review presented above, in an integrated system design, the condensation of anode exhaust gas would surely lead to heat loss. This highlights the importance of determining a proper condensation temperature for exhaust gas oxy-combustion to avoid undercooling. To do so, a burner that can reliably attain a satisfactory CO conversion rate is needed. It is therefore worth studying the amount of excess O_2 required to balance the flame stability, conversion rate, and CO_2 concentration. Exhaust gas should be burned around the equivalence ratio that leads to a high local flame temperature. In systems with long lifetimes, it is important to control the thermal creep deformation of the combustor liner, which is influenced by the inner jet flow and cooling strength. In contrast to an air combustor system, in this case, the oxidizer gas cannot be used directly as the liner cooling medium through a method such as film cooling (Topal et al. 2019) because the quantity of O_2 necessary for exhaust gas burning is rather small. Therefore, forced liner cooling must be implemented to reduce the liner temperature and CO conversion rate. However, the drivers of forced cooling increase the energy consumption of the system. Moreover, the high reaction temperature of oxy-combustion may lead to high levels of NO_x emissions because N_2 is present in both industrial syngas (Schluckner et al. 2020) and air separating oxygen (Khallaghi et al. 2020).

Most commercial flat-plate SOFC systems comprise fuel cell generation modules, which can be integrated by a few large stacks (e.g., FuelCell Company uses 12.5-kW stacks) or numerous small stacks (e.g., BloomEnergy Company uses 1 kW stacks). A system with a 10-kW gross power capacity could be considered as a modularization subsystem during the design of a system with either a single large stack or several small stacks. It would then be convenient to enlarge the system to 100 kW or even to the MW level. Therefore, in this article, a lab-scale anode exhaust gas concept was used to design and study an oxy-combustor for an IGFC system with a 10 kW gross power capacity through experiments and numerical simulations. The computational fluid dynamics (CFD) and chemical reactor network (CRN) methods were verified and applied to simulate the combustor's flame and emissions. The flame ignitions of exhaust gas and pure oxygen at various condensation temperatures were evaluated, and the effects of excess O_2 and liner cooling processes on the CO conversion rate were investigated. The impacts of jet flow and outside forced cooling conditions on the liner temperature were also analyzed. Finally, the pollutant emissions were studied for various anode processing conditions, i.e., different amounts of excess O_2. The results reported herein are valuable for developing IGFC systems integrated with CO_2 capture capabilities.

2 Experimental setup

Figure 1 shows the lab-scale exhaust gas concept for an oxy-combustor that consists of a flame chamber, a flame stabilizer, an oxygen swirler, and a fuel swirling jet. All components were made of high-temperature steel. The tangential angle of the fuel jet was 25°. The swirlers and stabilizer generated a swirling flow field and back flow that improved the mixing process and supported a stable flame root. Chilled air entered the cooling chamber to cool the flame chamber liner. The experimental operating conditions are shown in Table 1; these can be considered as typical conditions for the exhaust gas from a gross 10 kW IGFC system exhaust gas. The difference in species mole fractions might be caused by different fuel utilizations or system process designs. The Reynolds number of the combustor jet was approximately 1.5×10^5, meaning that the flow status in the flame chamber corresponded to fully-developed turbulence. This made it convenient to enlarge the combustor for systems larger than 10 kW because the flow field and flame shape were steady at higher Reynolds numbers (Wang et al. 2016a).

A schematic diagram of the test rig is shown in Fig. 2, wherein the modeled exhaust gas composed of H_2, CO, and CO_2 was taken as the fuel. All component gases were directly supplied by standard compressed gas cylinders with purity of 99.999%. Flow rates of these gases were adjusted by computer operated Alicat mass flow

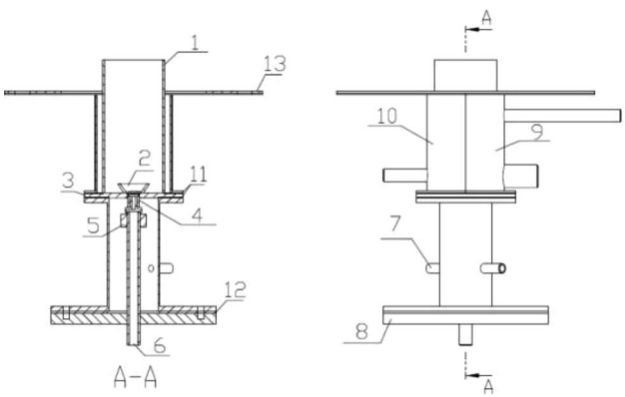

Fig. 1 Exhaust gas concept for an oxy-combustor for a 10-kW IGFC system. 1: flame chamber; 2: flame stabilizer; 3: oxygen swirler; 4: fuel swirler; 5: connector; 6: fuel pipe; 7: oxygen pipe; 8: base plate; 9–10: cooling air chambers; 11–13: sealing materials

Table 1 Operating conditions for the exhaust gas combustor experiments

Case	Flow rate (kg/h)	O_2 flow rate (kg/h)	Exhaust gas mole fractions			
			CO	H_2	H_2O	CO_2
1	3.48	0.47	0.069	0.197	0.061	0.673
2	3.48	0.69	0.091	0.261	0.061	0.587
3	3.45	0.45	0.101	0.169	0.061	0.669

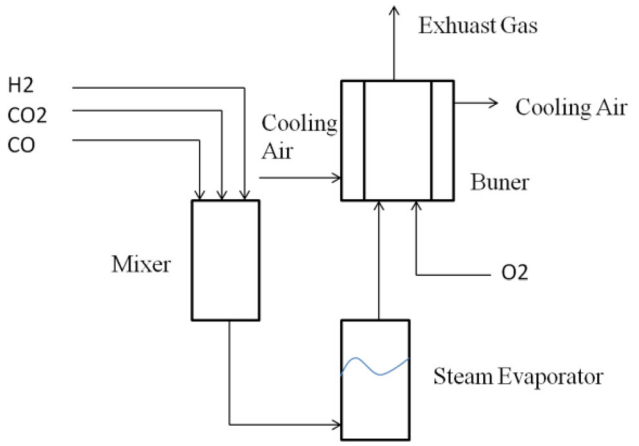

Fig. 2 Exhaust gas combustion test rig

controllers, whose accuracy was ± 2% measuring scales, to ensure the species proportions in the modeled exhaust gas. First, gases were mixed in a mixer with a heating function, and then the mixture regarded as fuel entered a steam evaporator from the bottom. Saturated vapor filled the space at the top of the evaporator. The fuel, together with the vapor, traveled through the evaporator and entered the combustor. During this process, the mole fraction of steam in the fuel could be adjusted by modifying the temperature of the evaporator. The burned flue gas was discharged to atmosphere at temperature about 515 K after water-cooling. Back pressure of the test rig was kept atmospheric pressure by a variable frequency fan. In this test, other slightly-inert components were replaced by CO_2. Cool air traveling through the cooling chamber could induce the forced convective cooling of the liner, and the convective coefficient could be controlled by altering the air flow rate. Exhaust gas was burned with pure oxygen inside the combustor, and a Testo 320 industrial gas analyzer with a drying function was used to measure the CO_2, O_2, and CO content in the flue gas. The analyzer was accurate to within 1% of the observed value for the main species and ± 1 ppm by volume (ppmv) for pollutants. To burn CO out, O_2 was supplied in an excess of 5%, while the temperature of the steam evaporator was held at 315 K. To avoid possible thermal interference, the species mole fraction was determined without external cooling air during experiments, so the cooling chamber could provide radiation protection. The air in the cooling chamber could therefore be considered as static. As a result, an approximately thermally-isolated environment was generated in the flame chamber.

3 Computational methods

3.1 CFD method

CFD modeling can provide comprehensive information during the design process, so a CFD method was used to simulate the flame inside the swirling combustor. The commercial software, Ansys Fluent 14.0, was used to solve the modeling equations. Some of our authors (Wang et al. 2015) previously established the high performance of the applied method by comparing various models and screening the obtained results according to experimental data. In subsequent studies, the model was further verified for Reynolds numbers ranging from 0.32×10^5 to 1.12×10^5 through experimental methods spanning various developed flow conditions (Wang et al. 2016a). A modified realizable k-ε turbulence model and an eddy dissipation concept (EDC) combustion model coupled with a detailed chemical mechanism were used, and an enhanced wall treatment was applied. The physical properties were calculated using the transport and thermal package in the chemical mechanism. The ideal gas law was adopted to compute the density of the gas, the specific heat was calculated based on the mixing law, and the thermal conductivity and kinematic viscosity were determined using the ideal gas mixing law. Kinetic theory was applied to calculate the mass and heat diffusivities. The radiation was simulated using a discrete ordinate (DO) model. Finally, the liner wall was set as a radiant and convective boundary (Wang et al. 2016a), and the combustor was modeled in three dimensions in the steady state.

To verify the CFD numerical method, a similar highly-reliable standard flame experiment was modeled. The methane-fueled burning experiment, which also involved a swirling diffusion flame jet, was carried out at Sydney University and described by Kalt et al. (2002). The temperature of the flame axis was measured to correlate these data with the flame structures. Case SM1 in those experiments was modeled using the aforementioned CFD method, and a GRI 3.0 scheme was applied to simulate the chemical reactions involved in methane combustion. The relationships between the flame temperature and the location on the central flame axis determined experimentally

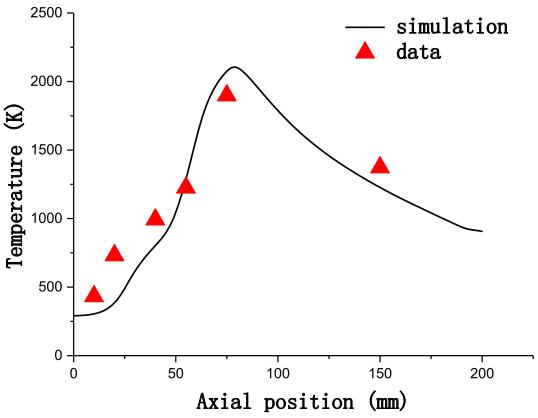

Fig. 3 Verification of CFD method

and via simulation are compared in Fig. 3, which reveals satisfactory agreement in terms of the flame structure.

The grid independence verification is presented in Fig. 4, which displays the temperature contours of the symmetry planes. Two series of mesh were used for these flame calculations; 2×10^5 cells or 1×10^6 cells were considered in the simulations presented in Fig. 4a and b, respectively. No notable differences were observed for these two mesh densities; therefore, 200,000-cell grids were used for further calculations to conserve computing resources.

3.2 Chemical reactor network method

A CRN model is typically used to simulate species and temperature fields in a combustor. This approach is advantageous because it can accurately calculate pollutant concentrations (i.e., NO_x and CO) and provide more information concerning the reaction by simulating finite-rate chemical transformations of combustion and pollutant formation based on detailed kinetic mechanisms. The reactor network must be constructed using a converged CFD simulation. To do so, the combustor volume is subdivided into a small number of connected reactors, and the mass fluxes through the network are determined from the CFD solution. Herein, a CRN model for the combustor was established according to the CFD results obtained as described in the previous section. The modeling process was developed, verified (Wang et al. 2016b), and applied (Shao et al. 2017) in previous reports, and the ultimate model is shown in Fig. 5. Perfectly-stirred reactor (PSR) models were used upstream to simulate the fuel/oxygen unmixedness in the primary zone; downstream reactors simulated the developing zone. The resident time was determined by the flow velocity, and mass transfer among the reactors was calculated based on elemental conservation. A detailed and previously verified (Wang et al. 2016b) chemical mechanism involving a syngas combustion scheme and a NO_x chemistry scheme was adopted in this study. Compared with model A (Fig. 5a), model B (Fig. 5b) was more detailed and contained more reactors to simulate each flame zones. The CRN models were solved using the commercial software, Chemkin 9.0. Simulated and experimental CO emission data are compared in Fig. 6, and the close agreements between the computational and experimental results indicate the reliability of the model. Additionally, no notable difference was observed between the model A and model B results. Therefore, in the subsequent studies, model A was employed to conserve computing resources, and the species components of Case 3 were considered, unless otherwise noted.

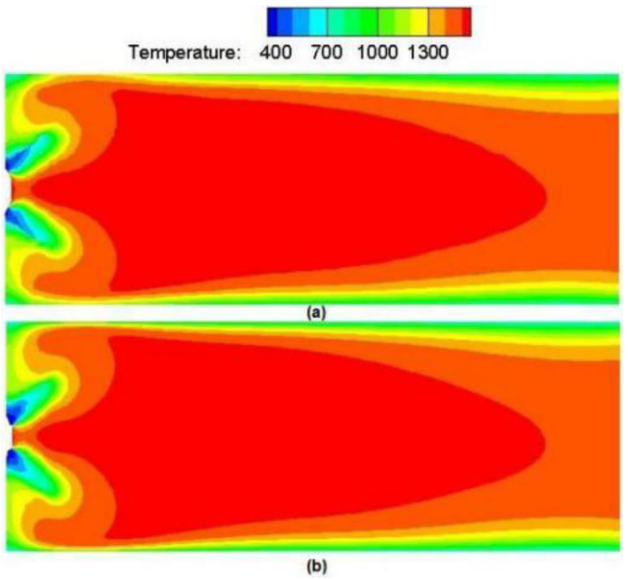

Fig. 4 Temperature distribution determined by CFD for different mesh densities: **a** 200,000 cells; **b** 1,000,000 cells

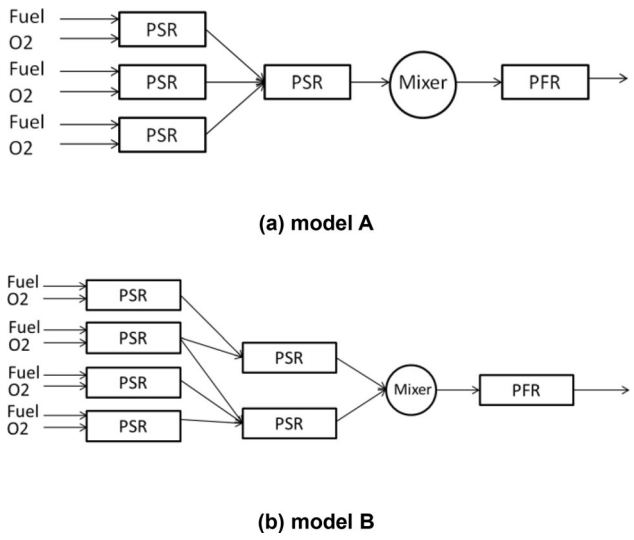

Fig. 5 Chemical reactor network models for the combustor

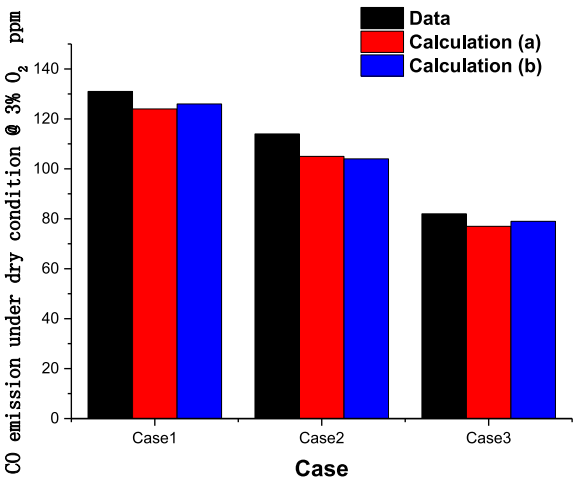

Fig. 6 Comparison between calculated and experimental results

4 Results and discussion

4.1 Exhaust gas condensation temperature effects on ignition

The moisture level in anode exhaust gas can be extremely high, which makes it difficult to obtain a steady flame in the combustor, primarily because some radical decomposition products of H_2O suppress the syngas burning reactions. Therefore, in IGFC systems, anode exhaust gas must be condensed before oxy-combustion to remove water. The heat loss from condensation can be recovered by a designated heat-recovering process, in which case, the partial pressure of steam at the entrance of the combustor is determined by the saturated vapor pressure. The condensation temperature (T_{con}) could therefore be considered as the inlet temperature of the combustor. A single PSR model was used to study the relationship between the condensation temperature and the flame temperature (Fig. 7), which is crucial for the flame stability. The

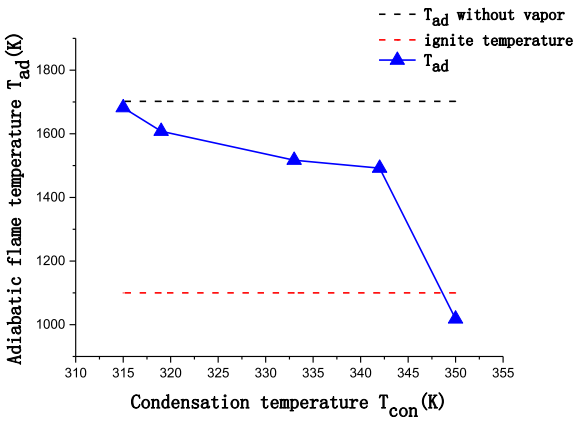

Fig. 7 Equivalence adiabatic flame temperature of exhaust gas as a function of various condensation temperatures

ignition temperature was set to 1100 K, and the resident time was 1 s.

The equivalence adiabatic flame temperature (T_{ad}) decreased as the condensation temperature increased (Fig. 7) because the moisture content was low at low condensation temperatures. When the condensation temperature exceeded 350 K, the flame temperature was lower than the ignition temperature, meaning that the excess steam prevented ignition. In practical systems, steam cannot be completely removed, so T_{ad} is always lower than the theoretical value without vapor. Under completely dry conditions, T_{ad} is around 1700 K for Case 3. Considering the heat loss during the burning process, it might be appropriate for T_{ad} to be 500 K higher than the ignition temperature to obtain a steady flame. Based on these results, 315 K was deemed the ideal condensation temperature for a system where $T_{ad} \approx 1680$ K; these conditions could be attained by using a water chiller.

4.2 CO conversion

The most important indicator for an exhaust gas treatment device aimed at CO_2 capture is the processing capacity, which is related to the dry CO_2 mole fraction in the exhaust gas after burning. Following combustion, the CO conversion could be determined by the flame temperature and quantity of oxidant. Both the equivalence ratio and the heat loss directly affect the flame temperature. As mentioned previously, forced convection was implemented outside the flame chamber to control the temperature of the liner, and this feature should certainly intensify the heat release problem. The CFD method was used to calculate the CO_2 mole fraction after treatments involving various equivalence ratios and liner air cooling convective coefficients. The cooling air temperature was set to 298 K. The Nusselt number (Nu) was determined from the Dittus-Boelter correlation (Eq. (1)) for a fully-developed flow, based on the Reynolds number (Re) calculated using Eq. (2):

$$\mathrm{Nu} = 0.023 Re^{0.8} \mathrm{Pr}^{0.4} \tag{1}$$

$$Re = \frac{\rho q d}{\mu A} \tag{2}$$

where, Pr is the Prandtl number, ρ is the density, q is the mass flow rate, d is the equivalence diameter, μ is the viscosity, and A is the sectional area. The results of simulations are shown in Fig. 8, and the data from the experiment described above are presented in Table 2.

Figure 8 indicates that the mole fraction of CO_2 after burning in dry conditions was ≥ 0.958 for every tested case. The remainder of the dry flue gas mainly consisted of CO, O_2, and other impurity gases. This suggested that the developed combustor system performed well for treating

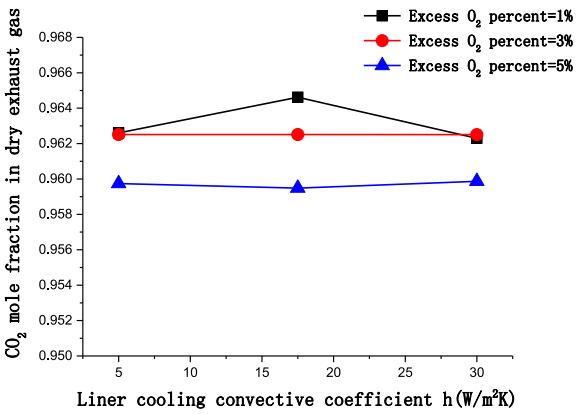

Fig. 8 Mole fraction of CO_2 in dry exhaust gas after burning (CFD calculations)

Table 2 Experimental data regarding CO_2 mole fractions in dry exhaust gas after burning

Case	CO_2 mole fraction
1	0.962
2	0.962
3	0.958

exhaust gas. The cooling convective coefficient appears to have a minor impact on CO conversion, which may be related to the small influence of heat loss on the flame temperature. In contrast, the CO mole fraction clearly varied as the degree of excess O_2 changed. This result confirmed that CO could almost be fully converted under the applied flame burning conditions. Excess O_2 decreased the mole fraction of CO_2 in the flue gas because it did not participate in the reaction. Instead, taking the unexpected unmixedness at jet outlets into consideration, excess O_2 facilitated CO burning out and reduced CO emissions. From this perspective, a 5% excess of O_2 was recommended since it did not clearly affect the CO_2 mole fraction after burning. The liner forced cooling strength had little influence on CO conversion. Table 2 shows that the mole fraction of CO_2 in dry flue gas after burning was ≥ 0.958, which could be considered an ideal rate for CO_2 capture; the CO_2 would be dried before the capture process. Overall, it was experimentally confirmed that CO could be converted to CO_2 efficiently via oxy-combustion.

4.3 Liner temperature

The temperature of the combustor liner is another key indicator by which to evaluate the oxy-combustion process. The liner temperature is strongly influenced by the flame temperature distribution. The equivalence ratio may vary within a narrow range for an oxy-combustor designed for CO_2 capture, which contribute to a relatively small flame temperature range, especially for a diffusion flame. Therefore, the flame temperature distribution depends primarily on the fuel jet form. As mentioned previously, forced air cooling should be implemented outside the liner, in which case, the liner temperature would be influenced by heat transfer and jet flow form. Heat flowed in from the high-temperature gas burning process and was then transferred out to the air-cooled outer chamber. For anode exhaust gas characterized by an extremely low calorific value, strong swirling movement may orient the flow field to stabilize the flame. Similarly, a tangentially angled fuel jet would influence the mass and heat transfer inside the liner because the fuel flow rate could be more than five times greater than the oxygen flow rate. Moreover, a tangential jet influences the mixedness of fuel and oxygen, which may affect the local flame temperature. The maximum liner temperature was calculated using the CFD model applying various outside convective coefficients and fuel jet tangential angles (Fig. 9). The O_2 flow rate at the boundary was set to 5% excess.

The maximum liner temperature decreased as the outer convective coefficient decreased, thus confirming that forced convection outside the flame chamber was an effective way to protect the combustor. It was observed that the maximum liner temperature reached an optimal value at a tangential angle of approx. 25°. The main reason for this could be as follow. Stronger swirling induced better mixing conditions. When the jet tangential angle was around 20°, the mixing of fuel and oxygen was not desirable. Furthermore, a high degree of unmixedness caused the flame to burn at a low equivalence ratio, which resulted in a high local temperature; the liner temperature increased when the local temperature was high. When the jet tangential angle was around 30°, the larger centrifugal force caused the high-temperature gas to scour the liner more

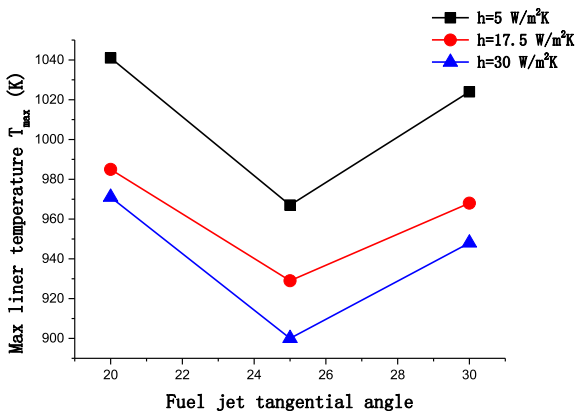

Fig. 9 Maximum temperature of the combustor liner under various conditions (CFD calculations)

severely, which caused a high liner temperature, albeit a more desirable degree of mixing. These results indicated an optimal tangential angle, which could vary with the dimensions of the combustor and allow control of the liner temperature.

4.4 Pollutant emissions

Pollutant emission is another key indicator for all kinds of power plants. In contrast to traditional plants, electrochemical reactions inside SOFCs have the potential to cut pollutant formation during fuel utilizing. However, oxy-combustion adds a burning step that could cause some emission problems. In general, O_2 production from a cryogenic air separation unit (ASU) can contain up to 5% N_2 by volume. Therefore, in practical IGFC systems, some N_2 is always present in syngas, even if O_2 gasification technology is involved. As a result, combustion pollution primarily consists of CO and NO_x. The aforementioned CRN model, which was established according to CFD results for a 25° jet swirl angle, was used to compute the pollutant emissions of the designed oxy-combustor. To do so, Case 2 and 3 were computed and compared, and it was determined that the fuel utilization ratio of Case 2 was lower than that of Case 3 because Case 2 contained more combustible components; this led to the observed difference between their exhaust gas compositions. The exhaust gas contained 3% N_2 by volume in the simulation case, and the ratio of the other components remained unchanged. The pollutant emissions were then computed with different excess quantities of O_2 under thermally-isolated conditions (similar to the experiment). Additionally, combustion processes with pure O_2 and with industrial O_2 containing 5% N_2 were compared to determine the impact of oxygen purity on NO_x and CO emissions; the results are presented in Figs. 10 and 11 for Case 3 and 2, respectively. It was considered that H_2 was completely converted to water following direct flame burning because H_2 has an extremely high burning rate compared with CO, especially under pure oxygen conditions. To enable meaningful comparisons between calculations, all of the results have been corrected to correspond to 3% O_2 concentration under dry conditions.

Both CO and NO_x emissions decrease with increasing excess of O_2. It is known that NO_x formation is directly related to the flame temperature. When there was only a small amount of excess O_2, the local flame temperature was higher, thus leading to higher NO_x emissions. On the other hand, a larger excess of O_2 caused CO to burn more completely, thus reducing CO emissions. Therefore, excess O_2 favored pollution reduction. Considering these relationships, if the CO_2 concentration met the requirements for CO_2 capture, the O_2 supply should be as high as

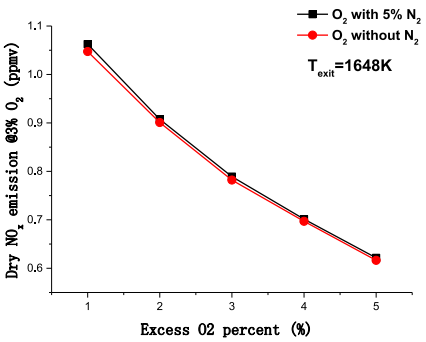

(a) NO_x emissions

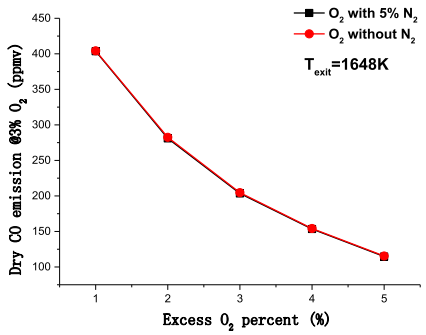

(b) CO emissions

Fig. 10 **a** NO_x and **b** CO pollutant emissions of Case 3 computed using the CRN model

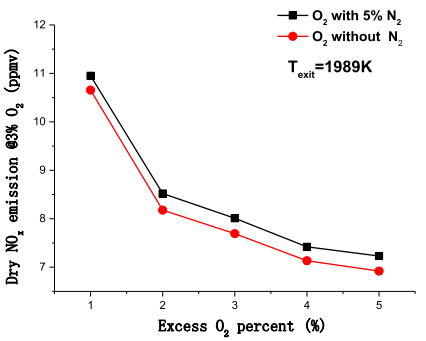

(a) NO_x emissions

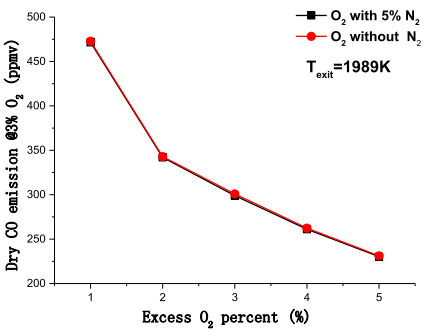

(b) CO emissions

Fig. 11 **a** NO_x and **b** CO pollutant emissions of Case2 computed using the CRN model

possible. The exit temperature of the combustor could be regarded similarly because the difference as a function of excess O_2 was not significant. In Case 2, more CO and NO_x were released than in Case 3 because Case 2 had a lower total utilization rate in fuel cells, which indicated that its exhaust gas contained more combustible components. Additionally, the flame temperature in Case 2 was approx. 2000 K, whereas it was 1650 K in Case 3; a high temperature leads to high NO_x emissions. Case 2 also contained more H_2, so the mole fraction of H_2O was high after burning. Vapor and H_2 in fuel prevent CO conversion to CO_2, especially at high temperature, which leads to high CO emissions (Wang et al. 2016a, b). The main reason for this phenomenon is that the vapor had a large heat capacity and reduced the flame temperature. Additionally, hydrogen radicals suppressed CO conversion through the reaction, $CO + OH \leftrightarrow CO_2 + H$. The experimental data presented herein were consistent with this concept. Furthermore, it is known that NO_x formation increases significantly when the temperature exceeds 1800 K. It could therefore be concluded that to design an environmentally friendly system, the total fuel utilization should be high enough to control the oxygen flame temperature of the anode exhaust gas below 1800 K. The NO_x emissions increased and the CO emissions decreased slightly as the oxygen purity decreased; however, the impact of oxygen purity on the NO_x and CO emissions was not significant. This was mainly because the oxygen flow rate was relatively small compared with that of the exhaust gas. Thus, the introduction of N_2 with the oxygen flow was small enough not to have a significant influence on the total N_2 concentration. Because N_2 did not participate in CO oxidizing reactions, no major distinctions were observed under different O_2 purity conditions.

Liner cooling can also affect pollutant emissions, so the NO_x and CO emissions were calculated for Case 2 under various cooling conditions (Fig. 12). Liner cooling protects the flame chamber from damage due to high temperatures; however, it also decreases the flame temperature inside the chamber. The combustor exit temperature with a convective coefficient of 17.5 W/m^2 generally decreased compared with that of the heat isolation case. The reduction in reaction temperature led to lower CO and higher NO_x emissions.

5 Conclusions

In this study, an oxy-combustor was evaluated through experiments and simulations (CFD and CRN methods) under various system processing conditions; the numerical methods were verified by experimental data. Several key indicators of combustor performance, including the

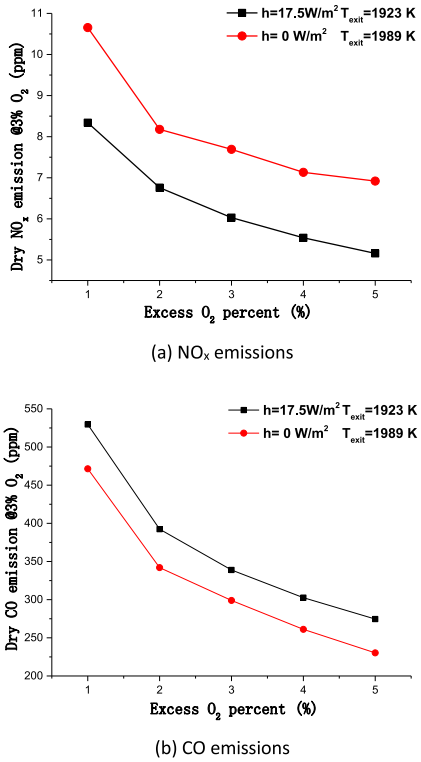

Fig. 12 **a** NO_x and **b** CO pollutant emissions of Case 2 computed using the CRN model

impacts of exhaust gas condensation temperature on flame ignition, CO conversion, liner temperature, and pollutant emissions, were discussed, and the main conclusions are as follows:

First, the anode exhaust gas should be condensed to remove water prior to oxy-combustion. For Case 3, which contained the least H_2, the T_{ad} value in dry conditions was approximately 1700 K. Considering the heat loss in a practical system, 315 K was determined to be the ideal condensation temperature for a system where T_{ad} was approx. 1680 K. This is a key parameter to consider when designing IGFC systems with integrated CO_2 capture processes.

Second, the mole fraction of CO_2 after burning under dry conditions was ≥ 0.958 when O_2 was in up to 5% excess. The determined convective coefficients indicated a slight effect on the CO conversion process. It was confirmed that CO was almost completely converted in the proper flame burning conditions and unreactive excess O_2 decreased the mole fraction of CO_2. A 5% excess of O_2 was therefore recommended to promote CO burning without significantly impacting the CO_2 mole fraction after burning. The forced cooling of the liner had little influence on CO conversion. These results confirmed that direct flame burning provided an effective and reliable way to

achieve CO_2 concentration in an IGFC, indicating that such oxy-combustors could be applied in industrial systems.

Additionally, for an oxy-combustor designed for CO_2 capture, the total range of flame temperatures was relatively small because the exhaust gas was essentially burned at a very low equivalence ratio to achieve CO_2 capture. The liner temperature was influenced by outward heat transfer as well as the jet form. Forced convection outside the flame chamber was demonstrated to be an effective way to protect the combustor. When the jet tangential angle was small, a high level of unmixedness between fuel and oxygen led to a high temperature, whereas when the jet tangential angle was large, the centrifugal force caused the high-temperature gas to scour the liner more severely. The maximum liner temperature reached an optimal value at a jet tangential angle of approx. 25°. These conclusions can therefore guide combustor design.

Finally, it was observed that both CO and NO_x emissions decreased with increasing excess of O_2. When there was only a small excess of O_2, more NO_x species were released because of the high flame temperature. In contrast, excess O_2 promoted more complete CO combustion. If the CO_2 concentration could meet the CO_2 capture requirement, the O_2 supply should be as high as possible. The purity of O_2 barely influenced the pollutant emissions. However, intense cooling of the liner decreased the flame temperature, which led to lower CO and higher NO_x emissions. Overall, to design an environmentally friendly system based on the relationships discussed herein, the total fuel utilization must be high enough to maintain the oxygen flame temperature of the anode exhaust gas lower than 1800 K.

Author contributions All authors contributed to the study conception and design. Material preparation, data collection and analysis were performed by Hanlin Wang, Qilong Lei, Pingping Li, Changlei Liu, Yunpeng Xue, Xuewei Zhang, Chufu Li, and Zhibin Yang. The first draft of the manuscript was written by Hanlin Wang and all authors commented on previous versions of the manuscript. All authors read and approved the final manuscript.

Funding This work was supported by the National Key R&D Program of China (No. 2017YFB0601900).

Declarations

Conflicts of interest The authors have no conflicts of interest to declare that are relevant to the content of this article.

References

Al-Khori K, Bicer Y, Koc M (2020) Integration of solid oxide fuel cells into oil and gas operations: needs, opportunities, and challenges. J Cleaner Product 245:118924

Chen X, Xu Z, Yang F, Zhao H (2019) Flame spray pyrolysis synthesized CuO-TiO_2 nanoparticles for catalytic combustion of lean CO. Proc Combust Instit 37:5499–5506

Dey S, Dhal GC (2020) Property and structure of various platinum catalysts for low-temperature carbon monoxide oxidations. Mater Today Chem 16:100288

Ferreira T, Wuillemin Z, Faulwasser T, Salzmann C, Van Herle J, Bonvin D (2019) Enforcing optimal operation in solid-oxide fuel-cell systems. Energy 181:281–293

Francisco J, Alvarez G, Gonzalo de Grado J (2016) Study of a modern industrial low pressure turbine for electricity production employed in oxy-combustion cycles with CO2 capture purposes. Energy 107:734–747

Han SW, Kim HD, Jeong M, Park KJ, Kim YD (2016) CO oxidation catalyzed by NiO supported on mesoporous Al2O3 at room temperature. Chem Eng J 283:992–998

Ilbas M, Bektas A, Karyeyen S (2019) A new burner for oxy-fuel combustion of hydrogen containing low-calorific value syngases: an experimental and numerical study. Fuel 256:115990

Imteyaz BA, Nemitallah MA, Abdelhafez AA, Habib MA (2018) Combustion behavior and stability map of hydrogen-enriched oxy-methane premixed flames in a model gas turbine combustor. Int J Hydrogen Energy 43:16652–16666

Kalt P, Al-Abdeli Y, Masri A, Barlow R (2002) Swirling turbulent non-premixed flames of methane: flow field and compositional structure. Proc Combust Inst 29(1):1913–1919

Khallaghi N, Hanak DP, Manovic V (2020) Techno-economic evaluation of near-zero CO2 emissions gas-fired power generation technologies: A review. J Nat Gas Sci Eng 74:103095

Li B, Shi B, Zhao X, Ma K, Xie D, Zhao D, Li J (2018) Oxy-fuel combustion of methane in a swirl tubular flame burner under various oxygen contents: operation limits and combustion instability. Exp Thermal Fluid Sci 90:115–124

Ning D, Wang S, Fan A, Yao H (2018) A numerical study of the effects of CO2 and H2O on the ignition charachteristics of syngas in a micro flow reactor. Int J Hydrogen Energy 43:22649–22657

Pirasaci T (2019) Non-uniform, multi-stack solid oxide fuel cell (SOFC) system design for small system size and high efficiency. J Power Sources 426:135–142

Rashwan SS, Ibrahim AH, Abou-Arab TW, Nemitallah MA, Habib MA, (2017) Experimental study of atmospheric partially premixed oxy-combustion flames anchored over a perforated plate burner

Schluckner C, Gaber C, Landfahrer M, Demuth M, Hochenauer C (2020) Fast and accurate CFD-model for NOx emission prediction during oxy-fuel combustion of natural gas using detailed chemical kinetics. Fuel 264:116841

Shao W, Zhao Y, Liu Y, Wang H, Tian Y, Lu Y, Zhang Z, Xiao Y (2017) Investigation of fuel/air mixing uniformity in a natural gas premixed burner for gas turbine combustor applications. Proc CSEE 3:795–802 ((**in Chinese**))

Spallina V, Nocerino P, Romano MC, Annaland MS, Campanari S, Galluci F (2018) Integration of solid oxide fuel cell (SOFC) and chemical looping combustion (CLC) for ultra-high efficiency power generation and CO_2 production. Int J Greenhouse Gas Control 71:9–19

Thallam-Thattai A, Oldenbroek V, Schoenmakers L, Woudstra T, Aravind P (2017) Towards retrofitting integrated gasification combined cycle (IGCC) power plants with solid oxide fuel cells (SOFC) and CO_2 capture—a thermodynamic case study. Appl Therm Eng 114:170–185

Topal A, Turan O (2019) One dimensional liner temperature prediction in a tubular combustor. Energy 171:1100–1106

Wang H, Lei F, Shao W, Xiong Y, Zhang Z, Xiao Y (2015) Screening and modification of CFD models for syngas turbine combustor. Proc CSEE 6:1429–1435 ((**in Chinese**))

Wang H, Lei F, Shao W, Zhang Z, Liu Y, Xiao Y (2016a) Experimental and numerical studies of pressure effects on syngas combustor emissions. Appl Therm Eng 102:318–328

Wang H, Shao W, Lei F, Zhang Z, Liu Y, Xiao Y (2016b) Experimental and numerical studies of pressure effects on syngas combustor liner temperature. Appl Therm Eng 82:30–38

Wang X, Lv X, Weng Y (2020) Performance analysis of a biogas-fueled SOFC/GT hybrid system integrated with anode-combustor exhaust gas recirculation loops. Energy 197:117213

Wu Z, Zhu P, Yao J, Tan P, Xu H, Chen B, Yang F, Zhang Z, Ni M (2020) Thermo-economic modeling and analysis of an NG-fueled SOFC-WGS-TSA-PEMFC hybrid energy conversion system for stationary electricity power generation. Energy 192:116613